Journal of Climate

Internal and forced interdecadal variations of global sea surface temperature in recent warming era

--Manuscript Draft--

Manuscript Number:	
Full Title:	Internal and forced interdecadal variations of global sea surface temperature in recent warming era
Article Type:	Article
Corresponding Author:	Dong-Ping Wang Stony Brook University Stony Brook, NY UNITED STATES
Corresponding Author's Institution:	Stony Brook University
First Author:	Dong-Ping Wang
Order of Authors:	Dong-Ping Wang
	Dake Chen
	Minghua Zhang
Abstract:	The roles of forced and natural modes of variability in the observed climate of the recent warming era are examined with extended empirical orthogonal function (EEOF) analysis of sea surface temperature (SST) in a single global domain with no detrending. The global nonseasonal SST variability since the mid-twentieth century can be described by the interannual El Nino - Southern Oscillation (ENSO) modes, an interdecadal oscillation mode, and a secular mode. The canonical ENSO mode indicates a regime shift in 1976/1977. The internal interdecadal oscillation shows the classical Atlantic Multidecadal Oscillation (AMO) pattern but accompanied with covarying SST anomalies in the extratropical North Pacific. The secular mode shows a widespread warming in the western Pacific and the Atlantic and Indian Oceans, but a cooling in the eastern Pacific. Moreover, about 70% of the global mean SST warming trend is explained by the secular mode alone. This suggests the possibility that the recent cooling trend in the eastern Pacific is externally forced, as opposed to the prevailing view of it as an internal cycle of the Pacific interdecadal variability.
Suggested Reviewers:	

Cover Letter

Click here to download Cover Letter: jclimate cover letter.doc

SoMAS
School of Marine and Atmospheric Sciences

Stony Brook University, Stony Brook, NY 11794-5000

Dong-Ping Wang, Professor Emeritus

Dear Editor,

Attached please find a manuscript, " Internal and forced interdecadal variations of global sea surface temperature in recent warming era", by Dong-Ping Wang, Dake Chen and Minhghua Zhang. The work examines the global SST patterns to identify the natural and externally forced variability. The study suggests the possibility that the recent cooling trend in the eastern Pacific is externally forced, as opposed to the prevailing view of it as an internal cycle of the Pacific interdecadal variability. We appreciate your consideration for publication in the *Journal of Climate*. Thanks.

Dong-Ping Wang

Internal and forced interdecadal variations of global sea surface temperature in recent warming era

Dong-Ping Wang[1,2], Dake Chen[2,3], Minghua Zhang[2]

email: dong-ping.wang@stonybrook.edu

[1] State Key Laboratory of Satellite Ocean Environmental Dynamics, Second Institute of Oceanography, Hangzhou, China
[2] School of Marine and Atmospheric Sciences, Stony Brook University, Stony Brook, New York, USA
3 Lamont-Doherty Earth Observatory, Columbia University, Palisades, New York, USA

Abstract

The roles of forced and natural modes of variability in the observed climate of the recent warming era are examined with extended empirical orthogonal function (EEOF) analysis of sea surface temperature (SST) in a single global domain with no detrending. The global nonseasonal SST variability since the mid-twentieth century can be described by the interannual El Nino - Southern Oscillation (ENSO) modes, an interdecadal oscillation mode, and a secular mode. The canonical ENSO mode indicates a regime shift in 1976/1977. The internal interdecadal oscillation shows the classical Atlantic Multidecadal Oscillation (AMO) pattern but accompanied with covarying SST anomalies in the extratropical North Pacific. The secular mode shows a widespread warming in the western Pacific and the Atlantic and Indian Oceans, but a cooling in the eastern Pacific. Moreover, about 70% of the global mean SST warming trend is explained by the secular mode alone. This suggests the possibility that the recent cooling trend in the eastern Pacific is externally forced, as opposed to the prevailing view of it as an internal cycle of the Pacific interdecadal variability.

1. Introduction

The global sea surface temperatures (SST) have large spatial and temporal variability (for a review, see Deser et al. 2010). On the interannual time scale, El Nino - Southern Oscillation (ENSO) is the dominant mode of global SST variability. For the interdecadal time scale, the Pacific Decadal Oscillation (PDO) and the Atlantic Multidecadal Oscillation (AMO) are the two principal basin-scale oscillations. Over a still longer time scale, the global mean temperature has risen steadily, which is attributed to external (anthropogenic) forcing of greenhouse gases. A major goal in climate diagnostics is to isolate the externally forced response in the presence of a large internal (natural) interdecadal variability (Thompson et al. 2009). The task can be quite daunting. For example, since the turn of the century the global warming trend has stalled unexpectedly. The warming 'hiatus' is thought to be triggered by a persistent cooling in the eastern equatorial Pacific (Kosa and Xie 2013; England et al. 2013). However, whether the cooling trend is part of a natural interdecadal cycle or is itself externally forced is not clear (Held 2013).

The empirical orthogonal function analysis (EOF) and its variations, which attempt to extract the largest spatio-temporal covariance of a data matrix, are commonly used to identify the dominant patterns of global or regional SST variability. For example, ENSO is the leading EOF mode of the detrended SST anomalies over the global ocean, and PDO and AMO are respectively the leading EOF modes of the North Pacific (20^{o}N - 70^{o}N) and the North Atlantic SST anomalies, after removing the global mean (Enfield et al. 2001; Ting et al. 2009; Deser et al. 2010). In analysis of the century long SST record, a secular trend often is removed. This is to minimize the impact of a strong warming trend in the early twentieth century, which otherwise might compromise the integrity of the leading EOF modes (Zhang et al. 1997). The assumption of a

58 homogeneous secular trend however is difficult to justify (Guan and Nigam 2008; Messie and
59 Chavez 2011).

60 In this study, we apply extended EOF (EEOF) analysis to global SST data without prior
61 detrending. Our analysis is limited to the post-1950 period, thus mainly dealing with the recent
62 rapid warming era which started in the mid-1970s. We note that the spatial pattern of the
63 warming trend in the early twentieth century differs substantially from that of the recent era.
64 Whether this is indicative of a changing climate or is an artifact of limited data coverage in the
65 early period is not clear. As EOF assumes a stationary spatial pattern, restricting analysis period
66 to a single warming era of primary interest seems prudent. We show that the global interdecadal
67 SST variability since the mid-twentieth century is mainly associated with a regime shift, a
68 covarying SST variability in the North Atlantic and the North Pacific, and a secular trend. The
69 individual SST pattern is also clearly reflected in the corresponding sea level pressure (SLP)
70 variation. The rest of the paper is organized as follows. Section 2 outlines the data and EEOF
71 method, section 3 describes the global SST pattern, global mean temperature, and global SLP
72 pattern, and section 4 discusses some key implications.

73 **2. Data and Methods**

74 *a. Data*

75 The gridded SST reanalysis is from the monthly UK Met Office Hadley Centre's sea ice and sea
76 surface temperature dataset, HadISST, a $1^o \times 1^o$ high-resolution SST dataset reconstructed from
77 in situ and satellite observations (Rayner et al. 2003). The study period is from 1950 to the
78 present. Seasonal means are computed from monthly data, and SST anomalies are formed by
79 removing the seasonal cycle, the mean of each season. The gridded SSTs are area weighted by
80 the square root of the cosine of latitude (North et al. 1982). The analysis is over the globe

between 70^oS and 70^oN, retaining the original 1^o data resolution. The gridded atmospheric reanalysis is from the monthly National Centers for Environmental Prediction/National Center for Atmospheric Research (NCEP/NCAR) Reanalysis for sea level pressure (SLP) and surface wind (Kalnay et al. 1996). The horizontal resolution is $2.5^o \times 2.5^o$, and the data is from 1948 to the present.

b. Methods

An extended empirical orthogonal function analysis (EEOF) is used in this study. EEOF is the same as EOF or the Principal Component Analysis, except that the original and its time-lagged fields are concatenated to form an extended dataset. This allows spatial patterns to evolve to capture the spatio-temporal variations. We use a sliding window of 5 seasons. Our analysis method is similar to Guan and Nigum (2008, 2009). The extended dataset is large, 252 seasons of 360 (longitudes) × 180 (latitudes) × 5 (lags) pixels each. For computational efficiency, a two-dimensional PCA, the Generalized Low Rank Approximation of Matrices (GLRAM), is adopted in this study (Ye 2005).

3. Results

a. Global patterns

The first 5 EEOF modes explain 19.2, 13.5, 7.6, 4.5, and 3.9% of total variance respectively. The EEOF modes are well separated according to North et al. (1982). Figure 1 shows the principal components (PCs) together with Nino-3.4. The Nino-3.4 index is the area averaged SST anomaly in the central-eastern tropical Pacific (5^oN-5^oS, 170^o-120^oW); for consistency, Nino-3.4 is smoothed over 5 seasons. It is seen that PC1 is well correlated with Nino-3.4, and PC3 and PC5 also display large interannual variations. PC2, on the other hand, has a secular trend, while PC4

shows a clear interdecadal oscillation. Also, in PC1, there is a sudden transition of the baseline in the mid-1970s.

Figures 2 show the base functions of the three primary modes exhibiting obvious changes in interdecadal time scales: the first, second, and the fourth modes, and Fig. 3 the secondary modes of interannual variability: the third and fifth modes. Figure 4 shows the averaged spatial patterns of the three primary modes, mean over the five seasons; the sign of the first mode is reversed to show the cold phase. We note that the averaged spatial patterns agree well with those derived from the common EOF analysis.

The first mode is a global manifestation of the canonical ENSO. The base function describes the warm phase (El Nino), marked by a large warming in the central-eastern tropical Pacific and along the coasts of North and South America, a cooling in the extratropical North Pacific, and a warming in the tropical Indian and Atlantic Oceans. The evolution of El Nino is clearly displayed in the 5-season EEOF pattern. The warm event starts in spring (year 0) (top panel, Fig. 2a), reaches its peak in fall and winter, and diminishes in the following spring (year 1). PC1 also shows an abrupt baseline shift in 1976/1977, which has no counterpart in Nino-3.4. The sudden warming corresponds to the well documented 'regime shift' in the North Pacific (Mantua et al. 1997).

The second mode shows a strong cooling in the eastern tropical Pacific in a narrow strip between 5^{o}S-5^{o}N, a widespread warming spanning symmetrically from the western tropical Pacific to the extratropical North and South Pacific, and a broad warming in the Atlantic and Indian Oceans. The pattern is similar to ENSO but with some notable differences. For example, during ENSO the SST anomalies are negligible in the western tropical Pacific and extratropical South Pacific

but the cold tongue is broader in the eastern equatorial Pacific (Fig. 4). Moreover, PC2 has a clear secular trend which is not present in Nino-3.4: it is quiescent prior to the regime shift but rises rapidly afterwards. In other words, the North Atlantic and Indian Oceans are becoming warmer in the recent decades while the eastern equatorial Pacific is cooler. A warmer Indian Ocean is believed to be responsible for an apparent change of the relationship between ENSO and rainfall in Australia since the early 1970s (Nicholls et al. 1996).

The fourth mode is characterized by a broad zonal band of warm anomalies in the extratropical North Pacific (~ 40^{o}N), warm anomalies at the equator near the dateline, and a broad warming in the North Atlantic. The North Atlantic SST pattern of strong SST anomalies in the subtropics and south of Greenland can be identified with the AMO. PC4 also matches with the AMO time sequence of warm phases through the end of the 1960s and since the beginning of the 2000s and a cold phase in between (Deser et al. 2010; also see Fig. 5b). The extratropical North Pacific SST pattern, on the other hand, resembles the PDO. The AMO and PDO are typically treated as the two independent, interdecadal timescale basin oscillations. However, the North Atlantic and North Pacific SSTs tend to vary together in the most recent 'cycle' since the mid-twentieth century. We note that a similar inter-basin covarying SST pattern is found in the internal multidecadal component of several climate simulations (DelSole et al. 2011). Atmospheric teleconnections of AMO on North Pacific SST is also indicated in a controlled coupled climate model experiment (Zhang and Delworth 2007).

The third and fifth modes are confined to the Pacific (Fig. 3) and are of interannual time scales (Fig. 1). They have previously been identified with a biennial and a non-canonical mode respectively in an analysis of the Pacific SST variability (Guan and Nigam 2008). The biennial mode has a characteristic ENSO pattern of strong SST anomalies in the central-eastern equatorial

Pacific. However, unlike the canonical mode, the anomalies switch sign in less than 3 seasons, corresponding to a 2-year cycle (Rasmusson et al. 1990). The non-canonical mode has a strong meridional temperature gradient near the Inter-tropical Convergence Zone (ITCZ), and is closely related to the Pacific meridional mode (PMM) (Chiang and Vimont 2004). The positive phase of PMM was often found to be a precursor of ENSO (Chang et al. 2007). This can be seen in the 5-season EEOF panels that the winter SST maximum of the biennial mode (bottom panel, Fig. 3a) is preceded by the peak PMM in spring (2nd panel from the top, Fig. 3b).

b. Global mean temperature

The first two EEOF modes together explain about 33% of the global SST variance, yet they account for 65.7 and 28.1% of variance of the global mean SST, respectively; the area average is weighted by the cosine of latitude. In other words, practically all of the observed global mean SST change in the recent warming era can be explained by the two largest spatially coherent patterns. Figure 5a shows global mean SST and global mean of the second mode; the first mode is nearly equal to the difference between the two time series ($\gamma = 0.96$) (not shown). The global mean SST shows a quiescent period before the regime shift of 1976/1977, a rapid warming afterwards, and a hiatus since 2000. After subtracting of the first mode of predominant interannual variability, the regime shift is removed and the hiatus also becomes less apparent. We calculate the linear trend for the current warming era (1977 - present). For the (5-season averaged) global mean SST, the linear trend is 0.082 ± 0.011 ^{o}C per decade (95% confidence interval). The secular trend accounts for almost 70% of the global temperature rise in this period, 0.056 ± 0.009 ^{o}C per decade, indicating that it is likely forced by greenhouse warming.

The North Atlantic mean SST is dominated by the second and fourth modes, which contribute 38.6 and 35.8 % of total variance respectively. The second mode is responsible for the secular trend, whereas the fourth mode is responsible for the interdecadal oscillation. Figure 5b shows the (5-season averaged) AMO index and the North Atlantic mean of the fourth mode; recall that the AMO index is the North Atlantic mean SST minus the global mean. The two time series have nearly identical interdecadal variations, which reinforces the earlier assertion that the fourth mode is basically the AMO. The linear trend (1977 - present) for the North Atlantic mean SST is 0.206 ± 0.021 per decade (95% confidence interval), about 2.5 times of the global mean. About half of the North Atlantic warming is associated with the secular trend, 0.102 ± 0.016 ^{o}C per decade, and the other half with the interdecadal mode, 0.098 ± 0.012 ^{o}C per decade. We note that the spatial patterns are substantially different between the interdecadal mode and the secular mode (Fig. 4). For example, the secular mode shows a strong positive SST anomaly off the east coast of the U.S., whereas the interdecadal mode has a weak negative SST anomaly. Conversely, the interdecadal mode has much stronger SST anomalies south of Greenland.

The North Pacific (20^{o}N - 70^{o}N) mean SST is also dominated by the second and fourth modes, which contribute 27.1 and 30.2 % of total variance respectively. For the North Pacific, the interdecadal variability is typically described by the PDO, the leading EOF mode of SST anomalies over the North Pacific after removing the global mean. To compare with PDO index, we construct a North Pacific (NP) index as the sum of the second and fourth modes over the North Pacific, minus the global mean. Figure 5c shows the PDO index and the NP index (the sign of the PDO index is reversed). The two time series agree rather well. In particular, the well-publicized PDO phase changes of 1976/1977 and 1999/2000 are reproduced by the NP index.

c. Global sea level pressure

192 Figure 6 shows the regression patterns of (5-season averaged) sea level pressure (SLP) anomalies
193 with the first, second, and fourth modes. The region south of 30^{o}S is excluded to avoid off-scale
194 amplitudes over the Southern Ocean. For the canonical ENSO mode, the tropical Pacific SLP
195 shows the classical Southern Oscillation (SO) with positive SLP anomalies west of the dateline
196 and negative anomalies to the east. There is also a strong negative SLP anomaly in the
197 extratropical North Pacific, corresponding to a deeper Aleutian low over the Gulf of Alaska
198 (Alexander et al. 2002). The secular mode has a similar SLP pattern: a see-saw of reversing SLP
199 between the eastern and western tropical Pacific and a large SLP anomaly in the extratropics (the
200 sign is reversed from the first mode). However, the SLP anomalies over the Gulf of Alaska are
201 not as intense as in ENSO, and consequently, the meridional SLP gradient across the equatorial
202 Pacific is considerably weaker. In fact, there is a secondary SLP maximum at the equator near
203 160^{o}W, which coincides with the center of cold anomalies (Fig. 4b).

204 The SLP pattern of the interdecadal mode is indicated by a low pressure center in the subtropical
205 North Atlantic, a high pressure center over the Greenland, and another positive center in the Gulf
206 of Alaska. In the North Pacific, a positive SLP anomaly in the Gulf of Alaska reduces the surface
207 heat flux and Ekman heat transport, which could account for the extratropical warm anomalies
208 (Alexander et al. 2002). In the North Atlantic, the SLP pattern is comparable to the North
209 Atlantic Oscillation (NAO) (Hurrell 1995). A positive AMO phase corresponds to a weakened
210 atmospheric circulation, which is also consistent with surface forcing of warm anomalies.
211 However, most previous studies do not support a direct atmospheric forcing of AMO (Kushnir
212 1994; Dima and Lohmann 2007).

213 Zhang et al. (1997) compared the interdecadal differences of mean SST, SLP and surface winds
214 between 1950-1976 and 1977-1993. Trenberth and Fasullo (2013) made a similar comparison

between 1979-1998 and 1999-2012. The three epochs correspond respectively to the negative, positive, and negative phases of the PDO (the sign is reversed, Fig. 4c). It is argued that the epoch differences mainly reflect the PDO phase change. We update the calculations for the same three epochs, 1950-1977 (E1), 1977-1999 (E2), and 1999-2013 (E3). Figure 7 shows epoch differences for SLP; the corresponding wind and SST patterns can be found in the above mentioned references. The two difference maps look superficially similar, as both are marked by strong positive SLP anomalies over the Gulf of Alaska. However, when compared with SLP regression patterns (Fig. 6), E2-E1 is much closer to the canonical ENSO mode (the sign is reversed) while E3-E2 resembles the secular mode. As originally noted in Zhang et al. (1997), the epoch difference between E1 and E2 is due to the regime shift (Fig. 1b). The epoch difference between E2 and E3, on the other hand, is mainly associated with the secular trend (Fig. 1c), and the corresponding SLP pattern of a weak meridional gradient across the equator is clearly distinguished from E1-E2. We note that the recent SLP trend is also similar to E3-E2 (England et al. 2013).

4. Discussion

In this study, we show that the observed interdecadal SST variability since the mid-twentieth century is mainly associated with a regime shift in 1976/1977 (first mode), a covarying SST oscillation between the North Atlantic and the North Pacific (fourth mode), and a secular trend (second mode). Our analysis differs from most previous studies in that we retain the secular trend. The detrending, which is a common practice in global analysis, assumes that the global secular trend is more-or-less spatially homogeneous. Our analysis shows that, on the contrary, the secular trend has large spatial variations with even a sign reversal (Fig. 4b). Since the detrending does a poor job of removing the global trend, it in effect introduces noise into the EOF analysis.

238 The secular mode likely is driven by anthropogenic forcing associated with greenhouse gases. It
239 may seem counterintuitive that a uniform radiative heating could induce regional cooling, but
240 strong feedbacks between the tropical ocean and the atmosphere can cause responses with spatial
241 variations. One such mechanism is an ocean dynamical thermostat (Clement et al. 1996; Cane et
242 al. 1997). In the equatorial Pacific, the thermocline shoals eastward, and hence, surface warming
243 in the east is offset by upwelling of cold subsurface water. This creates an east-west SST
244 gradient, which can be reinforced through the Bjerknes feedback to produce a cooling in the
245 eastern equatorial Pacific. The atmospheric feedbacks however are not considered in the ocean
246 thermostat (Kucharski et al. 2011). In a warming climate, the Walker Circulation is expected to
247 become weakened, which would oppose the ocean thermostat (Held and Soden 2006; DiNezio et
248 al. 2013).

249 The AMO is generally thought to be associated with the Atlantic meridional overturning
250 circulation (MOC) (Delworth and Mann 2000). A delayed response to the high NAO index has
251 been suggested for the AMO phase change in the mid-1990s (Robson et al. 2012; Msadek et al.
252 2014). A sustained negative AMO from the early 1970s to the mid-1990s (Fig. 5b) corresponds
253 to a negative SLP anomaly or a deeper low pressure over the Greenland. This enhances surface
254 cooling, which could lead to increased deep water formation and a larger overturning circulation.
255 A strengthened MOC, on the other hand, would cause an increased poleward surface heat
256 transport, which counters surface cooling and drives AMO towards a positive (warm) phase. We
257 note that the direct observations of MOC only started since 2004 (Kanzow et al. 2010). It
258 remains difficult to verify the model hypothesis.

259 Our analysis gives an alternative to the prevailing view that the recent cooling in the eastern
260 equatorial Pacific is caused by Pacific natural (interdecadal) oscillations. Whether a cooler

eastern equatorial Pacific is externally forced or is due to internal oscillations will have important implications for climate forecast (Kosaka and Xie, 2013; England et al. 2013). It is though important to remind that the objective analysis is severely constrained by a relatively short instrument record and the likelihood of a changing climate. A process based study is needed to verify if an empirical mode is genuine, and to elucidate the dynamical response of the tropical Pacific Ocean to global warming (Clement and DiNezio 2014).

Acknowledgements

DC is supported by grants from National Key Basic Research Program of China (2013CB430302), National Natural Science Foundation of China (91128204), and the Office of Naval Research (N00014-12-1-0911). MZ is supported by the National Science Foundation and the Office of Biological and Environmental Research of the Department of Energy.

References

Alexander, M. A. and Coauthors, 2002: The Atmospheric Bridge: The influence of ENSO teleconnections on air-sea interaction over the global oceans. *J. Climate,* **15**, 2205-2231.

Clement, A. C., R. Seager, M. A. Cane, and S. E. Zebiak. 1996: An ocean dynamical thermostat. *J. Climate,* **9,** 2190–2196.

Cane, M. A. and Coauthors, 1997: Twentieth century sea surface temperature trends. *Science* **275**, 957-960 .

Chang, P., L. Zhang, R. Saravanan, D. J. Vimont, J. C. H. Chiang, L. Ji, H. Seidel, and M. K. Tippett, 2007: Pacific meridionalmode and El Niño–Southern Oscillation. Geophys. Res. Lett., 34, L16608, doi:10.1029/2007GL030302.

Clement, A., and P. DiNezio. 2014: The tropical Pacific Ocean - back in the driver's seat? *Science*, **343**, 976-978.

Delsole, T., M.K. Tippett, and J. Shukla. 2011: A significant component of unforced multidecadal variability in the recent acceleration of global warming. *J. Climate,*. **24,** 909–926.

Delworth T, Mann M. E., 2000: Observed and simulated multidecadal variability in the Northern Hemisphere. *Climate Dyn.* **16**:661–76

Deser C, Phillips AS, Hurrell JW. 2004. Pacific interdecadal climate variability: linkages between the tropics and the North Pacific during boreal winter since 1900. *J. Climate* **17**, 3109–3124.

Deser, C., M. A. Alexander, S.-P. Xie, and A. S. Phillips, 2010: Sea surface temperature variability: Patterns and mechanisms. *Annu. Rev. Mar. Sci.*, **2**, 115–143.

DiNezio, P.N., G.A. Vecchi, and A.C. Clement, 2013: Detectability of changes in the Walker circulation in response to global warming. *J. Climate,* 4038-4048.

Enfield, D. B., A. M. Mestas-Nunez, and P. J. Trimble, 2001: The Atlantic multidecadal oscillation and its relation to rainfall and river flows in the continental U.S. *Geophys. Res. Lett.*, **28**, 2077–2080.

England, M.H. et al. 2014: Recent intensification of wind-driven circulation in the Pacific and the ongoing warming hiatus. *Nature Clim. Change* **4**, 222-227.

Guan, B. and Nigam, S, 2008: Pacific sea surface temperatures in the twentieth century: An evolution-centric analysis of variability and trend. *J. Climate*, **21**, 2790-2809.

Guan B. and Nigam S, 2009. Analysis of Atlantic SST variability factoring inter-basin links and the secular trend: clarified structure of the Atlantic Multidecadal Oscillation. *J. Climate*, **22**:4228–4240.

Harrison D. E, and Larkin N. K., 1998: El Nino-Southern Oscillation sea surface temperature and wind anomalies, 1946–1993. *Rev. Geophys.*, **36**, 353–399.

Held, I. M., and B. J. Soden, 2006: Robust responses of the hydrological cycle to global warming. *J. Climate*, **19**, 5686–5699.

Held, I., 2013: The cause of the pause. *Nature*, **501**, 318-319.

Hurrell, J. W., 1995: Decadal trends in the North Atlantic Oscillation: Regional temperatures and precipitation. *Science*, **269**,676–679.

Kalnay, E., and Coauthors, 1996: The NCEP/NCAR 40-Year Reanalysis Project. *Bull. Amer. Meteor. Soc.*, **77,** 437–471.

Kanzow, T., et al. 2010: Seasonal variability of the Atlantic meridional overturning circulation at 26.5°N, *J. Clim*., 23(21), 5678-5698, doi:10.1175/2010JCLI3389.1.

Kosaka, Y. and Xie, S-P., 2013: Recent global-warming hiatus tied to equatorial Pacific surface cooling. *Nature*, **501,** 403-407.

Kucharski, F., Kang, I. S., Farneti, R. & Feudale, L. 2011: Tropical Pacific response to 20th century Atlantic warming. Geophys. Res. Lett. **38,** L03702.Kushnir, Y., 1994: Interdecadal variations in North Atlantic sea surface temperature and associated atmospheric conditions. *J. Climate,* **7,** 141–157.

Mantua N.J, Hare S.R, Zhang Y, Wallace J.M, and Francis R., 1997: A Pacific interdecadal climate oscillation with impacts on salmon production. *Bull. Am. Meteorol. Soc.* **78**, 1069–79.

Messie, M. and Chavez, F., 2011: Global modes of sea surface temperature variability in relation to regional climate indices. *J. Climate,* **24**:4314-4331.

Msadek, R. et al., 2014: Predicting a decadal shift in north Atlantic climate variability using the GFDL forecast system. *J. Climate,* **27**:6472-6496.

Nicholls N., B. Lavery, C. Frederiksen, and W. Drosdowsky. 1996: Recent apparent changes in relationships between the El Nino - southern oscillation and Australian rainfall and temperature. *Geophys. Res. Lett*., **23**, 3357-3360.

North, G. R., T. L. Bell, and Cahalan, R. F., 1982: Sampling errors in the estimation of empirical orthogonal function. *Mon. Wea. Rev.,* **110,** 669–706.

Rasmussen, E. M. and Carpenter, T. H., 1982: Variations in sea surface temperature and surface wind fields associated with the Southern Oscillation/El Niño. *Mon. Weath. Rev*. **110**, 354-384.

Rayner, N. A., and Coauthors, 2003: Global analyses of sea surface temperature, sea ice, and night marine air temperature since the late nineteenth century. *J. Geophys. Res*., **108**, 4407.

Robson, R. T. Sutton, K. Lohmann, D. M. Smith, and M. D. Palmer, 2012: Causes of the rapid warming of the North Atlantic Ocean in the mid-1990s. *J. Climate,* **25**, 4116–4134.

Thompson, D. W. J., Wallace, J. M., Jones, P. D. & Kennedy, J. J., 2009: Identifying signatures of natural climate variability in time series of global-mean surface temperature: Methodology and insights. *J. Climate*, **22**, 6120-6141.

Trenberth, K. E. and J.F. Fasullo, 2013: An apparent hiatus in global warming. *Earth's Future*, **1**, 19-32.

Ye, J., 2005: Generalized low rank approximations of matrices. *Machine Learning*, **61**, 167-191.

Zhang, R., and T. L. Delworth, 2007: Impact of Atlantic multidecadal oscillations on North Pacific climate variability. *Geophys. Res. Lett*., **34**, L23708.

Zhang Y, Wallace J. M, Battisti D.S., 1997: ENSO-like interdecadal variability. *J. Climate*, **10**, 1004–1020.

Figure legends

Figure 1. The Nino-3.4 index (^{o}C) and principal components (PCs) of the first five EEOF modes. The PCs are normalized. They are 19.2, 13.5, 7.6, 4.5, and 3.9% of total variance respectively.

Figure 2. Spatial patterns of the (a) first, (b) second, and (c) fourth EEOF modes. Each mode spans five seasons, and is normalized with respect to the maximum absolute amplitude of the five seasons.

Figure 3. Spatial patterns of the (a) third, (b) fifth EEOF modes. Each mode spans five seasons, and is normalized with respect to the maximum absolute amplitude of the five seasons.

Figure 4. The five-season averaged spatial patterns for the (a) first, (b) second, and (c) fourth EEOF modes. Each mode is normalized.

Figure 5. (a) Global mean SST (blue) and second EEOF mode (red); (b) AMO index (blue) and fourth EEOF mode (red); and (c) PDO index (blue) and sum of second and fourth EEOF modes minus global mean (red).

Figure 6. Sea level pressure regressed to the five-season averaged EEOF modes: (a) first, (b) second, and (c) fourth. Each mode is normalized. Contour interval is 0.2. The colored regions are above 95% confidence interval.

Figure 7. Interdecadal differences of sea level pressure between (a) 1950-1977 and 1977-1999, and (b) 1977-1999 and 1999-2013. Each map is normalized. Contour interval is 0.2.

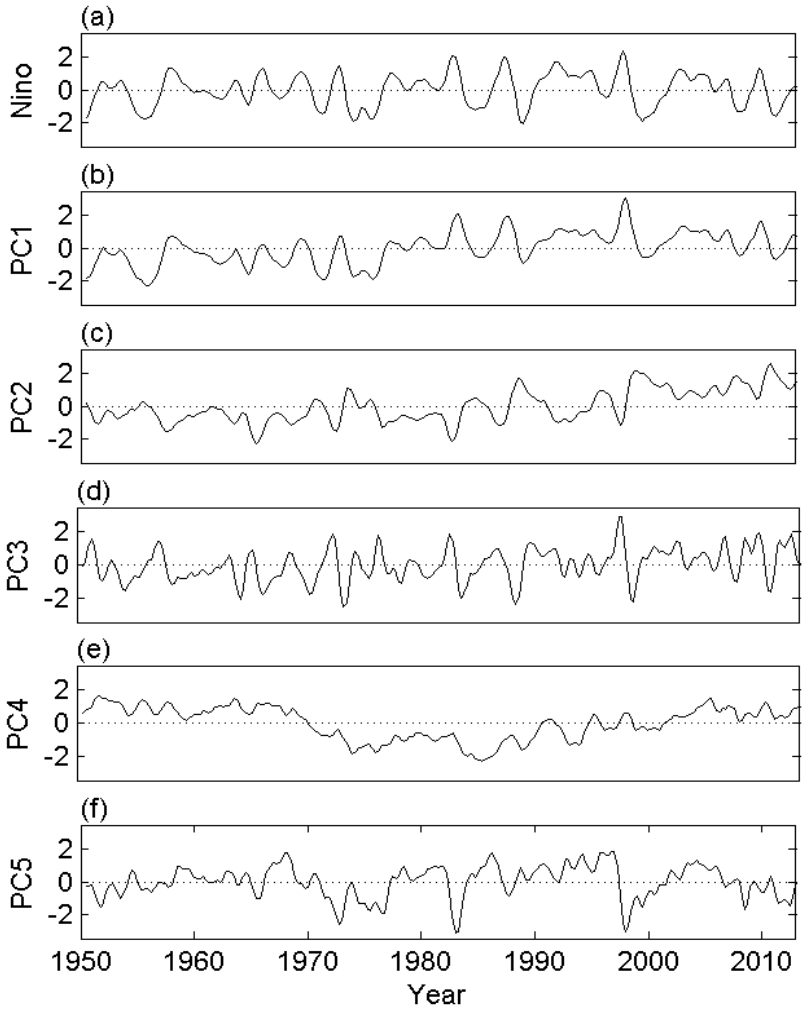

Figure 1. The Nino-3.4 index (^{o}C) and principal components (PCs) of the first five EEOF modes. The PCs are normalized. They are 19.2, 13.5, 7.6, 4.5, and 3.9% of total variance respectively.

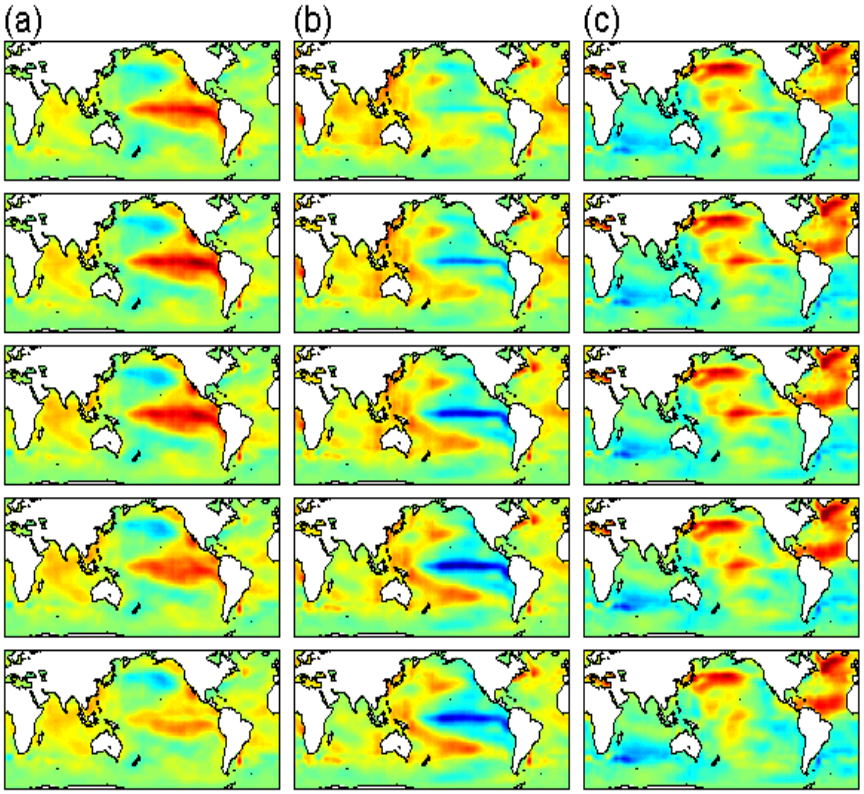

Figure 2. Spatial patterns of the (a) first, (b) second, and (c) fourth EEOF modes. Each mode spans five seasons, and is normalized with respect to the maximum absolute amplitude of the five seasons.

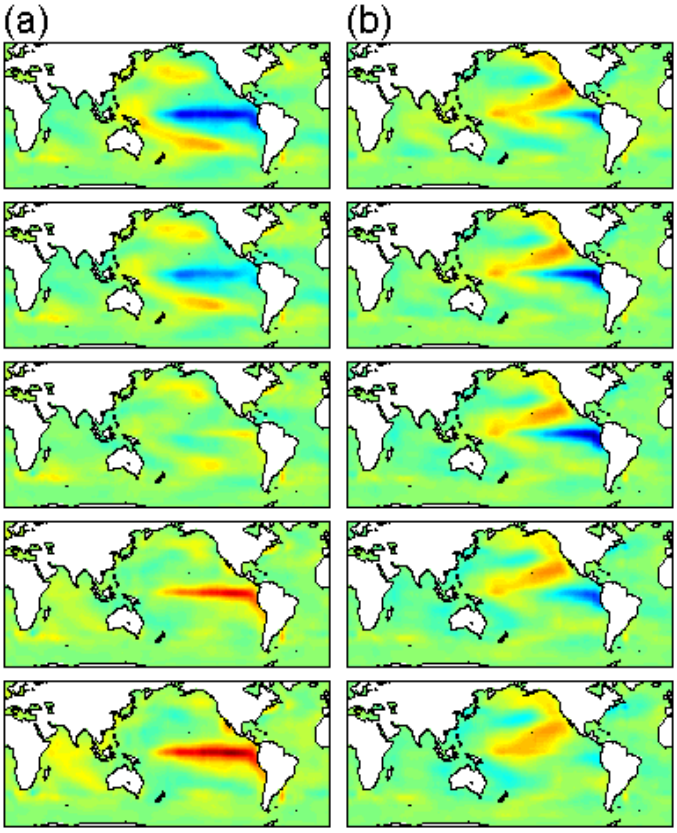

Figure 3. Spatial patterns of the (a) third, (b) fifth EEOF modes. Each mode spans five seasons, and is normalized with respect to the maximum absolute amplitude of the five seasons.

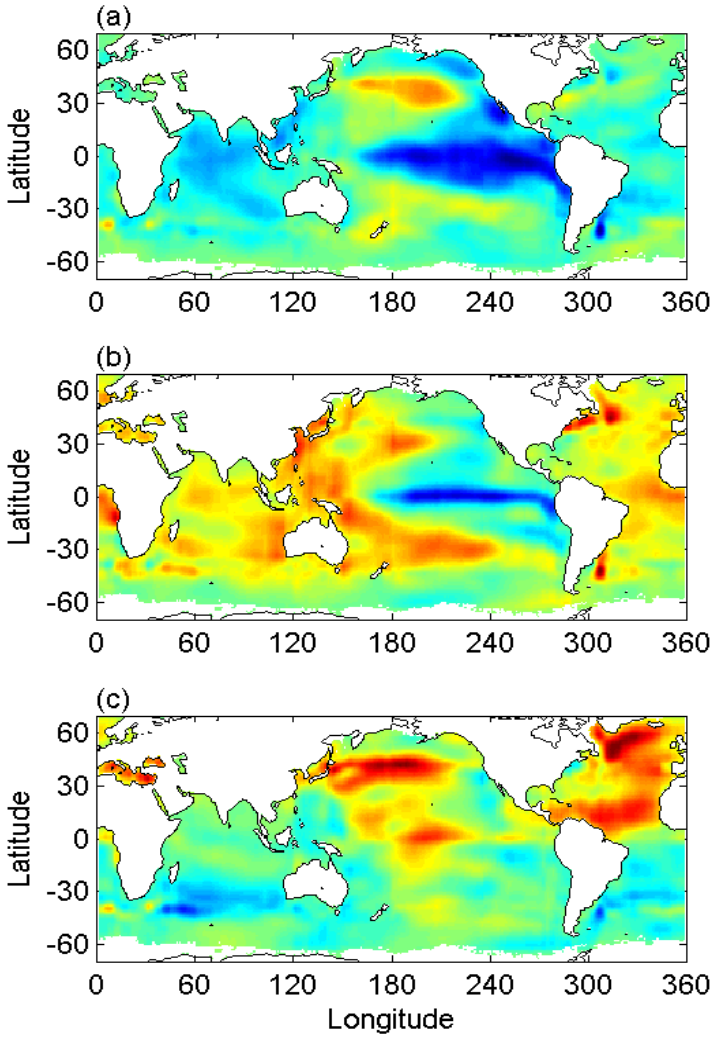

Figure 4. The five-season averaged spatial patterns for the (a) first, (b) second, and (c) fourth EEOF modes. Each mode is normalized.

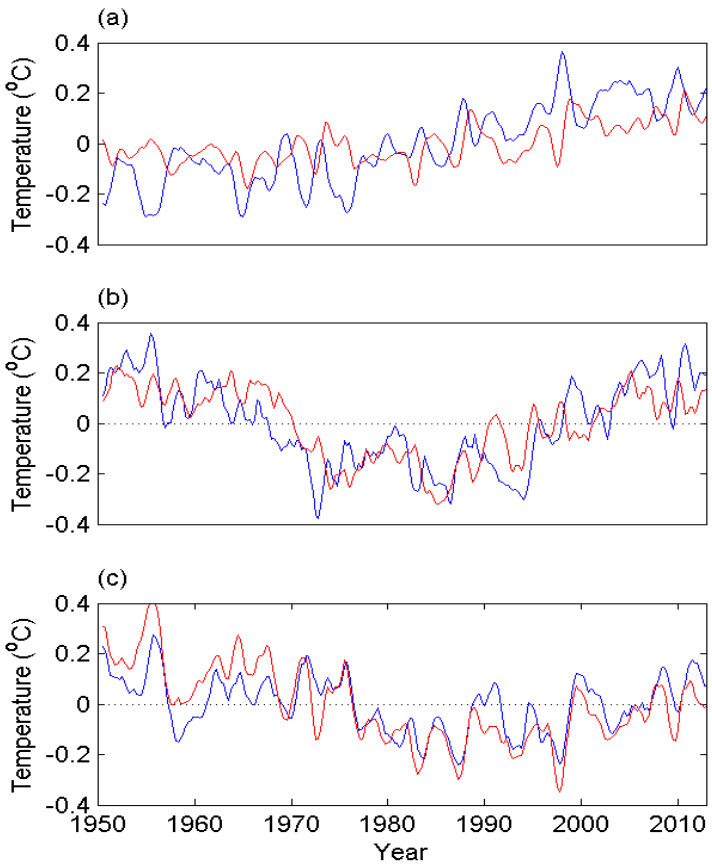

Figure 5. (a) Global mean SST (blue) and second EEOF mode (red); (b) AMO index (blue) and fourth EEOF mode (red); and (c) PDO index (blue) and sum of second and fourth EEOF modes minus global mean (red).

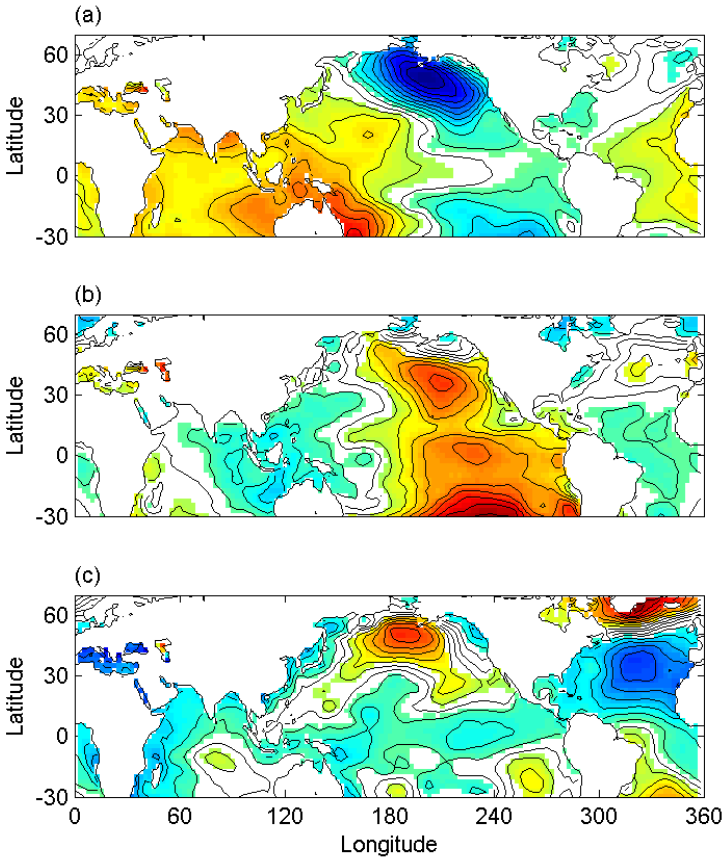

Figure 6. Sea level pressure regressed to the five-season averaged EEOF modes: (a) first, (b) second, and (c) fourth. Each mode is normalized. Contour interval is 0.2. The colored regions are above 95% confidence interval.

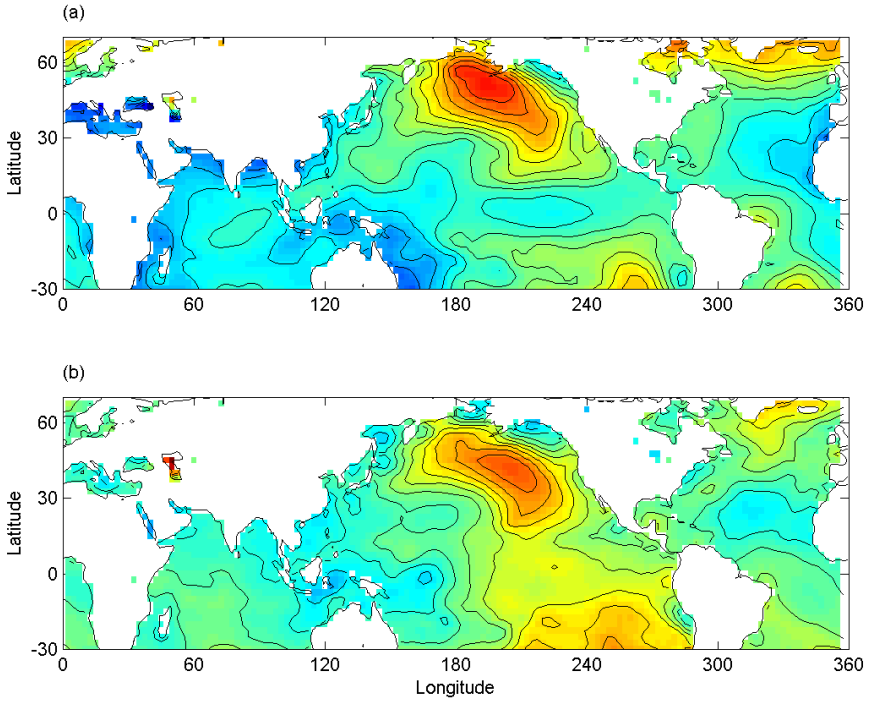

Figure 7. Interdecadal differences of sea level pressure between (a) 1950-1977 and 1977-1999, and (b) 1999-2013 and 1977-1999. Each map is normalized. Contour interval is 0.2.

Figure 1
Click here to download Non-Rendered Figure: fig1.png

Figure 2
Click here to download Non-Rendered Figure: fig2.png

Figure 3
Click here to download Non-Rendered Figure: fig3.png

Figure 4
Click here to download Non-Rendered Figure: fig4.png

Figure 5
Click here to download Non-Rendered Figure: fig5.png

Figure 6
Click here to download Non-Rendered Figure: fig6.png

Figure 7
Click here to download Non-Rendered Figure: fig7.png